Frontiers of Information Technology & Electronic Engineering
www.jzus.zju.edu.cn; engineering.cae.cn; www.springerlink.com
ISSN 2095-9184 (print); ISSN 2095-9230 (online)
E-mail: jzus@zju.edu.cn

Design and experimental validation of event-triggered multi-vehicle cooperation in conflicting scenarios*

Zhanyi HU[§1], Yingjun QIAO[§2,3], Xingyu LI[1], Jin HUANG[†‡1], Yifan JIA[†‡1], Zhihua ZHONG[2]

[1]*School of Vehicle and Mobility, Tsinghua University, Beijing 100084, China*

[2]*Chinese Academy of Engineering, Beijng 100088, China*

[3]*MOE Key Laboratory of Road and Traffic Engineering, Tongji University, Shanghai 200092, China*

[†]E-mail: huangjin@tsinghua.edu.cn; jiayifan@mail.tsinghua.edu.cn

Received Oct. 24, 2021; Revision accepted Mar. 14, 2022; Crosschecked May 25, 2022; Published online June 30, 2022

Abstract: Platoon control is widely studied for coordinating connected and automated vehicles (CAVs) on highways due to its potential for improving traffic throughput and road safety. Inspired by platoon control, the cooperation of multiple CAVs in conflicting scenarios can be greatly simplified by virtual platooning. Vehicle-to-vehicle communication is an essential ingredient in virtual platoon systems. Massive data transmission with limited communication resources incurs inevitable imperfections such as transmission delay and dropped packets. As a result, unnecessary transmission needs to be avoided to establish a reliable wireless network. To this end, an event-triggered robust control method is developed to reduce the use of communication resources while ensuring the stability of the virtual platoon system with time-varying uncertainty. The uniform boundedness, uniform ultimate boundedness, and string stability of the closed-loop system are analytically proved. As for the triggering condition, the uncertainty of the boundary information is considered, so that the threshold can be estimated more reasonably. Simulation and experimental results verify that the proposed method can greatly reduce data transmission while creating multi-vehicle cooperation. The threshold affects the tracking ability and communication burden, and hence an optimization framework for choosing the threshold is worth exploring in future research.

Key words: Connected and automated vehicles; Event-triggered control; Nonlinear and uncertain dynamics; Conflicting scenarios

https://doi.org/10.1631/FITEE.2100504 **CLC number:** U4; TP29

1 Introduction

Transportation activities are becoming more intense with increased vehicle ownership, which makes road transport more challenging. Equipped with sensing and communication apparatuses, connected and automated vehicles (CAVs) have great potential for improving traffic efficiency and road safety (Li SE et al., 2017). The widely studied platoon control is an effective strategy for coordinating CAVs (Zheng et al., 2016). In a typical platoon control system on highways, vehicles drive in the same lane with a compact formation at a harmonized longitudinal speed, which can be regarded as a one-dimensional (1D) case of multi-agent cooperation. Two-dimensional (2D) conflicting scenarios (such as generic intersections and intricate road geometry) and traffic protocols pose remarkable challenges to the application of platoon techniques.

In the 2D case, the main challenge is how to resolve the conflict relationship of approaching vehicles (Li W and Ban, 2020). Various approaches have

§ These authors contributed equally to this work
‡ Corresponding authors
* Project supported by the National Natural Science Foundation of China (Nos. 61872217, U20A20285, U1701262, and U1801263)
ORCID: Zhanyi HU, https://orcid.org/0000-0003-3335-8300; Yingjun QIAO, https://orcid.org/0000-0003-1602-5651; Jin HUANG, https://orcid.org/0000-0001-8774-2936; Yifan JIA, https://orcid.org/0000-0003-4411-8222

been reported in the literature for conflict-free passage in conflicting scenarios. The reservation-based approach was first proposed by Dresner and Stone (2008). It allocates tempo-spatial resources to approaching vehicles according to the "first come, first served" (FCFS) protocol to avoid collisions. Huang et al. (2012) proposed an intelligent intersection approach to improve the FCFS mechanism. In Huang et al. (2012)'s work, vehicles' arrival time was calculated according to their estimated driving mode, while all vehicles in the traditional FCFS protocol were simply assumed to have a constant speed. Planning-based methods were also developed to resolve potential collisions by eliminating trajectory overlaps. Specifically, Bian et al. (2020) proposed a trajectory optimization algorithm to enhance the safety and throughput of road transport. Furthermore, Dai et al. (2016) enhanced the passengers' quality of experience by optimizing vehicular movements for safely and efficiently negotiating an intersection. Mirheli et al. (2019) formulated the trajectory planning problem as vehicle-level mixed-integer nonlinear programs to minimize the travel time. In addition, the corresponding vehicle-level solutions were pushed towards global optimality by rendering consensus among vehicles. Although planning-based methods yield better performance, Rios-Torres and Malikopoulos (2017) pointed out that a satisfactory solution could be hard to obtain when dealing with a complex planning problem involving many CAVs. As a consequence, the potential of planning-based methods for real-world implementation has been impeded by such deficiencies (Meng et al., 2018).

Virtual platooning is a promising technique in coordinating CAVs in conflicting scenarios because it has less computational burden and can adapt to various situations. Uno et al. (1999) proposed the inventive virtual platooning concept to organize vehicles at highway on-ramps. Vehicles on the ramp road were projected to the main road, which transformed the 2D cooperation problem into a 1D case. Consequently, platoon control techniques are applicable to virtual platoon systems to avoid potential collisions and to maintain sufficient traffic throughput. Morales Medina et al. (2018) proposed an intersection management strategy based on virtual platooning. A vehicle would adopt the virtual cooperative adaptive cruise control (VCACC) strategy (or the CACC strategy) if a virtual (or physical) predecessor was detected. di Vaio et al. (2019) further developed and tested virtual platooning techniques at generic intersections. The stability of the virtual platoon system was analytically proved. Field tests with autonomous cars further validated the effectiveness of the proposed method.

The vehicular ad hoc network (VANET) is a key ingredient in platoon control systems for establishing vehicle-to-vehicle (V2V) communication, and virtual platoons are no exceptions. For example, the fifth-generation (5G) technologies have been applied to VANET. Shi et al. (2021) and Castiglione et al. (2021) did some pioneer work in 5G-based VANET. The time-triggered control (TTC) scheme has been widely used in existing platoon control methods. In TTC, vehicles exchange data at a fixed frequency. Data transmission is activated regardless of whether the driving state has changed, which creates excessive use of communication resources. Even worse, VANET suffers more imperfections and constraints (such as transmission delay and dropped packets) due to its multi-hop and infrastructure-less features when the communication burden increases (di Bernardo et al., 2015; Ge et al., 2018), which may jeopardize the stability of the multi-vehicle system. To secure a reliable VANET, it is important to make efficient use of scarce communication resources. To be more specific, only information that is required for the virtual platoon stability is transmitted.

The event-triggered control (ETC) scheme is such a resource-aware method that can achieve balance between communication efficiency and control performance. In ETC, the transmission instants are determined by a predefined triggering condition. Only when consecutively measured outputs change significantly does transmission occur (Li T et al., 2020). As a result, ETC has been applied to vehicle platoon control for efficient communication. For example, Dolk VS et al. (2017) developed an ETC scheme and a communication strategy. The $\mathcal{L}_2$ string-stable performance was analytically proved and was validated with on-road experiments. Guo et al. (2014) proposed a novel distributed ETC strategy. The triggering condition was examined periodically at constant sampling instants to avoid Zeno-behavior (an infinite number of events in finite time). ETC with a tunable threshold parameter was explored by Wen et al. (2018). Sufficient conditions for stabilizing the tracking error system subject to

time-varying delay were formulated. There are also ETC methods that take into account the features of practical platoon systems, such as sensor and actuator faults (Yue et al., 2017), packet losses (Dolk V and Heemels, 2017), and switching topologies (Shen et al., 2019). Ding et al. (2018) conducted a thorough survey of event-triggered consensus of multi-agent systems and the results revealed that the ETC scheme could reduce the use of wireless communication. For this reason, in this paper we aim to develop an ETC method that creates communication-efficient cooperation of CAVs in conflicting scenarios. Although various ETC methods that consider practical features are available in the literature, as far as the authors know, there have been few ETC results for virtual platoons subject to time-varying parametric uncertainty (i.e., uncertain platoon systems). Because the parametric uncertainty of practical vehicle dynamics also has a great influence on system stability, it is important to explore the integration of the ETC mechanism and uncertain platoon systems, which is the second motivation of this study.

In this study, a distributed ETC framework is proposed for coordinating CAVs in conflicting scenarios. The transmission of speed and acceleration information via VANET is governed by the triggering condition for efficient use of limited communication resources. The contributions of this paper are summarized as follows:

1. A distributed robust control protocol is proposed for multi-vehicle cooperation in conflicting scenarios. Different from existing studies (Morales Medina et al., 2018; di Vaio et al., 2019; Castiglione et al., 2021), the proposed method not only guarantees the stability of the virtual platoon system, but also reduces the communication burden using the ETC framework.

2. A new event-triggering condition is proposed to determine if relevant data should be transmitted. Different from the aforementioned studies (Guo et al., 2014; Dolk VS et al., 2017; Wen et al., 2018), in which only the state error was considered, the triggering condition in this paper integrates the state error with the bound of uncertainty so that the threshold can be estimated more precisely.

3. Most notably, the capability of the proposed distributed ETC in reducing the number of transmissions is experimentally validated using two self-driving vehicles in a VCACC scenario. This provides a concrete evidence of the superiority and possible practical implementation of the proposed method.

2 Problem statement and the proposed solution

2.1 Multi-vehicle cooperation in a conflicting scenario

A generic conflicting scenario composed of p entrances and q exits is defined as $C = \{\boldsymbol{S}, \boldsymbol{F}, R_{\mathrm{C}}\}$, where $\boldsymbol{S} = (p, q)$ stands for the basic structure and R_{C} is the communication range of the roadside agent (RA) that determines the passing sequence. Additionally, the coordinate system of the 1D virtual lane is represented by $\boldsymbol{F} = (\boldsymbol{O}, \boldsymbol{e})$, where $\boldsymbol{O}$ is the origin (i.e., the center of the conflicting area (CA)) and $\boldsymbol{e}$ is the positive direction pointing to the exit. Specifically, $\boldsymbol{S} = (2, 1)$ represents the merging scenario in highway on-ramps, while $\boldsymbol{S} = (1, 2)$ represents the diverging case. Moreover, $\boldsymbol{S} = (4, 4)$ represents a more complex conflicting scenario, i.e., a four-legged intersection.

Consider an intersection $\mathcal{C}_e = \{(4, 4), (\boldsymbol{O}, \boldsymbol{e}), R_{\mathrm{C}}\}$, which is shown in Fig. 1a. It is assumed that (1) overtaking is not allowed in real lanes, (2) each vehicle is capable of lateral path tracking, (3) vehicles can exchange information with others via a wireless network, and (4) the location information of all approaching vehicles is monitored and broadcast by the RA through infrastructure-to-vehicle (I2V) communication. The aim is that all approaching vehicles negotiate the CA safely and efficiently. On this basis, in this paper we intend to develop a communication-efficient control method based on an ETC framework.

2.2 Solution to the cooperation problem

The proposed solution is threefold. First, a virtual lane is constructed according to vehicles' distance to $\boldsymbol{O}$. Therefore, the 2D vehicle clusters are transferred into a 1D virtual platoon. The virtual lane of intersection $\mathcal{C}_e$ and the projection of the 2^{nd} and 4^{th} vehicles are presented in Fig. 1a. Then, the passing sequence manifested by a spanning tree is determined by the RA using the algorithm in Xu et al. (2018). Vehicles in adjacent depth maintain a desired car-following distance, while those in the same depth have no traffic movement conflicts with

each other and can traverse the intersection simultaneously. Finally, a robust distributed event-triggered controller is designed. The architecture of the proposed control framework is shown in Fig. 1b. The speed and acceleration of its predecessor p_i are measured by on-board sensors and transmitted to vehicle i via V2V communication. To make better use of limited communication resources, an additional triggering module (TM) with a pre-defined triggering condition will be applied to reduce the number of transmissions.

Remark 1 The proposed method is applicable to a generic conflicting scenario like highway on-ramps and intersections. This section adopts the four-legged intersection as an example to explain the proposed solution. The cooperation problem in other scenarios can be handled similarly.

3 Model description and control objectives

Consider the intersection shown in Fig. 1a and the corresponding virtual platoon composed of six vehicles in a VANET environment. First, the third-order vehicle dynamics is presented. Then, the triggering condition is introduced. Finally, the control objectives are proposed.

3.1 Nonlinear and uncertain dynamics

The longitudinal dynamics of the i^{th} vehicle is formulated in Eq. (1), where t is the time, x_i is the position, v_i is the speed, u_i is the input of the longitudinal dynamics, F_i is the longitudinal force, and M_i, $\bar{c}_i$, and τ_i are the vehicle mass, nominal value of aerodynamics coefficient, and inertial lag respectively. $\bar{f}_i = r_i M_i g\cos\theta + M_i g\sin\theta$ is the nominal resistance force, where r_i, θ, and g are the resistance coefficient, road slope, and gravity acceleration, respectively. The uncertainties in vehicle dynamics are denoted by $\Delta c_i\big(x_i(t), v_i(t), \sigma_i(t), t\big)$ and $\Delta f_i\big(x_i(t), v_i(t), \sigma_i(t), t\big)$, which are first-order continuously differentiable. The uncertain parameter is denoted as $\sigma_i \in \Sigma_i \subset \mathbb{R}^p$, where Σ_i is an unknown set and the set $\mathbb{R}^p$ is compact but unknown. In the rest of this paper, arguments are sometimes omitted when no confusion is likely to arise.

The longitudinal dynamics (1) can be simplified

$$\begin{cases} \dot{x}_i(t) = v_i(t), \\ \dot{v}_i(t) = \dfrac{1}{M_i}\Big[F_i(t) - \Big(\bar{c}_i + \Delta c_i\big(x_i(t), v_i(t), \sigma_i(t), t\big)\Big)v_i^2(t) - \Big(\bar{f}_i + \Delta f_i\big(x_i(t), v_i(t), \sigma_i(t), t\big)\Big)\Big], \\ \dot{F}_i(t) = \dfrac{1}{\tau_i}\big(-F_i(t) + u_i(t)\big). \end{cases} \tag{1}$$

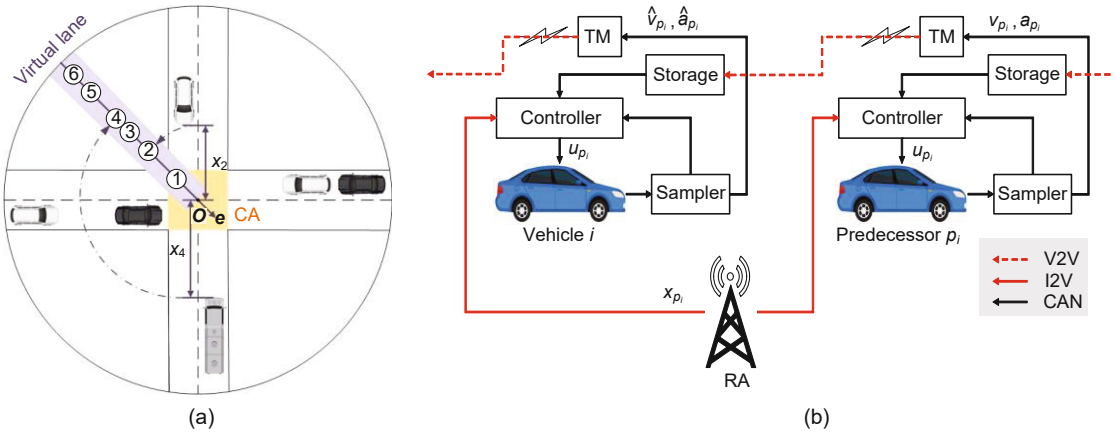

Fig. 1 Proposed solution: (a) layout of a four-legged intersection; (b) architecture of the event-triggered control framework. CA: conflicting area; TM: triggering module; RA: roadside agent; V2V: vehicle-to-vehicle; I2V: infrastructure-to-vehicle; CAN: controller area network. References to color refer to the online version of this figure

as

$$\begin{cases} \dot{x}_i = v_i, \\ \dot{v}_i = a_i, \\ \dot{a}_i = \dfrac{1}{M_i\tau_i}u_i - \dfrac{1}{\tau_i}a_i \\ \qquad -\dfrac{1}{M_i\tau_i}\left[\bar{c}_i(v_i^2 + 2\tau_i v_i a_i) + \bar{f}_i\right] + \Psi_i, \end{cases} \tag{2}$$

where a_i is the acceleration and

$$\Psi_i(v_i, a_i, t) = -\frac{1}{M_i\tau_i}\Big[\left(\Delta c_i v_i^2 + \Delta f_i\right) + \tau_i\left(\Delta\dot{c}_i v_i^2 + 2\Delta c_i v_i a_i + \Delta\dot{f}_i\right)\Big]. \tag{3}$$

Here, Ψ_i integrates the unknown but bounded uncertain portion.

3.2 Triggering condition

The triggering condition of the predecessor of vehicle i, namely vehicle p_i, is defined as

$$T_{j+1}^{p_i} = \inf_{t\in\mathbb{R}^+}\left\{t > T_j^{p_i} \mid \|\boldsymbol{\Phi}_{p_i}\boldsymbol{\xi}_{p_i}^{\mathrm{T}}(t)\| > \zeta_{p_i}\right\}, \tag{4}$$

where

$$\boldsymbol{\xi}_{p_i}(t) = \begin{bmatrix} v_{p_i}(T_j^{p_i}) - v_{p_i}(t) \\ a_{p_i}(T_j^{p_i}) - a_{p_i}(t) \\ \left(v_{p_i}(T_j^{p_i}) - v_{p_i}(t)\right)\Pi_i^2 \end{bmatrix}^{\mathrm{T}},$$

$T_j^{p_i}$ is the latest transmission time of vehicle p_i, $\boldsymbol{\xi}_{p_i}$ is the state deviation, ζ_{p_i} is the threshold of the triggering condition, $\boldsymbol{\Phi}_{p_i} = [\phi_{p_i,1}, \phi_{p_i,2}, \phi_{p_i,3}]$ is the weighing matrix, and $\phi_{p_i,1}$, $\phi_{p_i,2}$, and $\phi_{p_i,3}$ are positive constants. $\Pi_i(\cdot)$ is a known function associated with the uncertain portion Ψ_i. It is worth stressing that the sampling period of the control system is h ($h > 0$), and hence the transmission instants (i.e., $T_j^{p_i}$ and $T_{j+1}^{p_i}$) are all multiples of h. In other words, the transmission instants can be denoted as $T_j^{p_i} = q_j^{p_i}h$, where $j \in \mathbb{N}^+$ and $q_j^{p_i}$ is the sampling instant corresponding to the j^{th} triggering of vehicle p_i ($q_j^{p_i} \in \mathbb{N}^+$).

According to the triggering condition (4), for $t \in [T_j^{p_i}, T_{j+1}^{p_i})$, we have

$$\|\boldsymbol{\Phi}_{p_i}\boldsymbol{\xi}_{p_i}^{\mathrm{T}}(t)\| \le \zeta_{p_i}. \tag{5}$$

Remark 2 In practical implementation, a main problem for ETC is how to select an appropriate threshold ζ_i. A large ζ_i may jeopardize the tracking ability whereas a small ζ_i may not ease the communication burden. Hence, engineers tend to estimate ζ_i according to the bottomline of tracking ability (i.e., $v_{p_i}(T_j^{p_i}) - v_{p_i}(t)$ and $a_{p_i}(T_j^{p_i}) - a_{p_i}(t)$). However, the above state deviation can be caused by system uncertainty instead of the change in driving behavior. The proposed triggering condition (4) deals with this problem by combining the uncertainty-related function $\Pi_i(\cdot)$ so that engineers can estimate ζ_i more precisely.

3.3 Control objectives

The spacing between the i^{th} vehicle and its preceding vehicle is defined as

$$d_i(t) = x_{p_i}(t) - x_i(t) - L_{p_i}, \tag{6}$$

where $t = 0$ is the moment when the i^{th} vehicle enters the communication range. In addition, $x_{p_i}(t)$ and L_{p_i} are the position and length of vehicle p_i, respectively.

The constant time headway car-following policy is used, i.e.,

$$d_i^*(t) = q_i v_i(t) + d_{\mathrm{s}}, \tag{7}$$

where $d_i^*(t)$, $q_i > 0$, and $d_{\mathrm{s}} > 0$ are the desired spacing, time headway, and minimum allowable spacing, respectively.

Consequently, the spacing error can be denoted as

$$\begin{aligned} e_i(t) =& d_i^*(t) - d_i(t) \\ =& q_i v_i(t) + d_{\mathrm{s}} - x_{p_i}(t) + x_i(t) + L_{p_i}. \end{aligned} \tag{8}$$

The control objective of the virtual platoon is twofold. On one hand, the tracking error can converge to zero and stay within a small region around zero (i.e., uniformly bounded and uniformly ultimately bounded). On the other hand, the virtual platoon is string-stable with the proposed control. To better interpret the above objectives, we propose the following definitions:

Definition 1 (Uniform boundedness) If for any $y_i > 0$, there exists $\chi_i(y_i) < \infty$ such that if $\|\boldsymbol{\omega}_i(t_{\mathrm{B}})\| \le y_i$, then $\|\boldsymbol{\omega}_i(t)\| \le \chi_i(y_i)$ for all $t \ge t_{\mathrm{B}}$, then $\boldsymbol{\omega}_i(t)$ is affirmed to be uniformly bounded.

Definition 2 (Uniform ultimate boundedness) If for any $y_i > 0$ with $\|\boldsymbol{\omega}_i(t_{\mathrm{B}})\| \le y_i$, there exists $\underline{\chi}_i > 0$ such that $\|\boldsymbol{\omega}_i(t)\| \le \overline{\chi}_i$ for any $\overline{\chi}_i > \underline{\chi}_i$ as $t \ge$

$t_{\mathrm{B}}+T_i(\overline{\chi}_i,y_i)$, where $T_i(\overline{\chi}_i,y_i)<\infty$, then $\boldsymbol{\omega}_i(t)$ is affirmed to be uniformly ultimately bounded.

Definition 3 (String stability) If for any $y>0$, there exists $\eta>0$ such that if $\|\boldsymbol{e}_i(t_{\mathrm{s}})\|_\infty<\eta$, then $\sup_i\|\boldsymbol{e}_i(t)\|_\infty<y$ for all $t>t_{\mathrm{s}}$, then the platoon ($i\in\{1,2,\dots,n\}$) is affirmed to be string-stable at the equilibrium $\boldsymbol{e}_i=\boldsymbol{0}$.

4 Distributed control design and performance analysis

4.1 Robust control design

According to Eq. (8), the second-order derivative of the spacing error with respect to t can be written as

$$\ddot{e}_i=q_i\dot{a}_i+a_i-a_{p_i}. \tag{9}$$

By substituting Eq. (6) into Eq. (9), we obtain the dynamics of e_i, i.e.,

$$\begin{aligned}\ddot{e}_i=&q_i\Big[\frac{1}{M_i\tau_i}u_i-\frac{1}{\tau_i}a_i-\frac{1}{M_i\tau_i}\\&\cdot\left(\bar{c}_i(v_i^2+2\tau_iv_ia_i)+\bar{f}_i\right)+\Psi_i\Big]+a_i-a_{p_i}\\=&\frac{q_i}{M_i\tau_i}u_i+\Upsilon_i+q_i\Psi_i,\end{aligned} \tag{10}$$

where

$$\begin{aligned}\Upsilon_i=&-q_i\left[\frac{1}{\tau_i}a_i+\frac{1}{M_i\tau_i}\left(\bar{c}_i(v_i^2+2\tau_iv_ia_i)+\bar{f}_i\right)\right]\\&+a_i-a_{p_i}.\end{aligned} \tag{11}$$

The following lumped error is defined as

$$\beta_i=h_ie_i(t)+\dot{e}_i(t), \tag{12}$$

where $h_i>0$ is a weighing coefficient.

Next, the robust controller is designed as

$$\begin{aligned}u_i=-\frac{M_i\tau_i}{q_i}\left(h_i\hat{\dot{e}}_i+\hat{\Upsilon}_i+\kappa_i\hat{\beta}_i+\frac{2\mu_i\Pi_i}{|\mu_i|+\epsilon_i}\right),\\t\in[T_j^{p_i},T_{j+1}^{p_i})\end{aligned} \tag{13}$$

where κ_i and ϵ_i are positive scalar constants, and the parameters in the form of $\hat{(\cdot)}$ are denoted as

$$\begin{cases}\hat{\dot{e}}_i(t)=q_ia_i(t)+v_i(t)-v_{p_i}(T_j^{p_i}),\\\hat{\beta}_i(t)=h_ie_i(t)+\hat{\dot{e}}_i(t),\\\hat{\Upsilon}_i(t)=-q_i\Big[\frac{1}{\tau_i}a_i(t)+\frac{1}{M_i\tau_i}\\\qquad\cdot\Big(\bar{c}_i\left(v_i^2(t)+2\tau_iv_ia_i(t)\right)+\bar{f}_i\Big)\Big]\\\qquad+a_i(t)-a_{p_i}(T_j^{p_i}).\end{cases} \tag{14}$$

Additionally, $\mu_i=\hat{\beta}_i\Pi_i$ and Π_i is the bound of the uncertain portion in vehicle dynamics, which obeys the following legitimate assumption:

Assumption 1 (Chen and Zhang, 2010) For all $(v_i,a_i,t)\in\mathbb{R}^2\times\mathbb{R}^+$, $\sigma_i\in\Sigma_i$, there exists a known function $\Pi_i(\cdot):\mathbb{R}^2\times\mathbb{R}^+\to\mathbb{R}^2\times\mathbb{R}^+$ such that

$$\max_{\sigma_i\in\Sigma_i}|q_i\Psi_i(v_i,a_i,t)|\le\Pi_i(v_i,a_i,t). \tag{15}$$

As mentioned above, the uncertain elements Δc and Δf are bounded. In other words, $\Pi_i(\cdot)$ is used to represent the bound of the entire uncertain portion.

4.2 Stability analysis

We adopt the Lyapunov-Minmax method to analyze the stability of the controlled system under the proposed controller (13). The stability of the system is twofold. From the perspective of an individual vehicle, it is expected that the spacing error is uniformly bounded and uniformly ultimately bounded under the proposed controller. Besides, from the perspective of the multi-vehicle system, the virtual platoon is expected to achieve string stability.

Theorem 1 The lumped tracking error β_i of the uncertain error dynamical system (10) is uniformly bounded and uniformly ultimately bounded with the robust controller (13), and the virtual platoon is string-stable.

Proof Choose the following Lyapunov function candidate:

$$V_i(t)=\frac{1}{2}\beta_i^2(t),\ \forall t\in[T_j^{p_i},T_{j+1}^{p_i}). \tag{16}$$

Taking the derivative of Eq. (16) with respect to t ($t\in[T_j^{p_i},T_{j+1}^{p_i})$), we have

$$\begin{aligned}\dot{V}_i\overset{(12)}{=}&\beta_i(h_i\dot{e}_i+\ddot{e}_i)\\\overset{(10)}{=}&\beta_i\left(h_i\dot{e}_i+\frac{q_i}{M_i\tau_i}u_i+\Upsilon_i+q_i\Psi_i\right)\\\overset{(13)}{=}&\beta_i\left(h_i\dot{e}_i-h_i\hat{\dot{e}}_i-\hat{\Upsilon}_i-\kappa_i\hat{\beta}_i-\frac{2\mu_i\Pi_i}{|\mu_i|+\epsilon_i}+\Upsilon_i+q_i\Psi_i\right)\\=&-\kappa_i\beta_i^2+\underbrace{\beta_i\left(q_i\Psi_i-\frac{2\mu_i\Pi_i}{|\mu_i|+\epsilon_i}\right)}_{\chi_{i,1}}\\&+\underbrace{\beta_i\left[h_i(\dot{e}_i-\hat{\dot{e}}_i)+(\Upsilon_i-\hat{\Upsilon}_i)+\kappa_i(\beta_i-\hat{\beta}_i)\right]}_{\chi_{i,2}}.\end{aligned} \tag{17}$$

If $|\mu_i|>\epsilon_i$, we have

$$\begin{aligned}\chi_{i,1}&\overset{(16)}{<}\frac{\beta_i}{|\hat{\beta}_i|}|\hat{\beta}_i|\left(\Pi_i-\frac{2\mu_i\Pi_i}{|\mu_i|+|\mu_i|}\right)\\&=\frac{\beta_i}{|\hat{\beta}_i|}\left(|\mu_i|-\frac{\mu_i^2}{|\mu_i|}\right)\\&=0.\end{aligned}\tag{18}$$

Additionally, according to Eqs. (8), (11), and (14), we have

$$\begin{aligned}\chi_{i,2}=&\beta_i\left[h_i(\dot{e}_i-\dot{\hat{e}}_i)+(\Upsilon_i-\hat{\Upsilon}_i)+\kappa_i(\beta_i-\hat{\beta}_i)\right]\\=&\beta_i\Big[h_i\left(v_{p_i}(T_j^{p_i})-v_{p_i}(t)\right)\\&+\left(a_{p_i}(T_j^{p_i})-a_{p_i}(t)\right)+\kappa_i\left(v_{p_i}(T_j^{p_i})-v_{p_i}(t)\right)\Big]\\=&\beta_i\Big[(h_i+\kappa_i)\left(v_{p_i}(T_j^{p_i})-v_{p_i}(t)\right)\\&+\left(a_{p_i}(T_j^{p_i})-a_{p_i}(t)\right)\Big].\end{aligned}\tag{19}$$

According to the Cauchy–Schwarz inequality, Eq. (19) can be further scaled as

$$\begin{aligned}\chi_{i,2}\le&\frac{\kappa_i}{2}\beta_i^2+\frac{1}{2\kappa_i}\Big[(h_i+\kappa_i)\big(v_{p_i}(T_k^{p_i})-v_{p_i}(t)\big)\\&+\left(a_{p_i}(T_k^{p_i})-a_{p_i}(t)\right)\Big]^2\\\overset{(4)}{\le}&\frac{\kappa_i}{2}\beta_i^2+\frac{1}{2\kappa_i}\left[\left(\frac{h_i+\kappa_i}{\phi_{p_i,1}}\right)^2+\left(\frac{1}{\phi_{p_i,2}}\right)^2\right]\\&\cdot\left\|\boldsymbol{\Phi}_{p_i}\boldsymbol{\xi}_{p_i}^{\mathrm{T}}\right\|^2\\\overset{(5)}{\le}&\frac{\kappa_i}{2}\beta_i^2+\Omega_i\zeta_{p_i}^2,\end{aligned}\tag{20}$$

where $\Omega_i=\dfrac{1}{2\kappa_i}\left[\left(\dfrac{h_i+\kappa_i}{\phi_{p_i,1}}\right)^2+\left(\dfrac{1}{\phi_{p_i,2}}\right)^2\right]$.

By combining expressions (17), (18), and (20), we have

$$\dot{V}_i\le-\frac{\kappa_i}{2}\beta_i^2+\Omega_i\zeta_{p_i}^2.\tag{21}$$

Otherwise, $|\mu_i|\le\epsilon_i$, and we have

$$\begin{aligned}\chi_{i,1}&\overset{(16)}{\le}\beta_i\Pi_i\left(1-\frac{\mu_i}{\epsilon_i}\right)\\&=\beta_i\Pi_i-\frac{\beta_i\hat{\beta}_i\Pi_i^2}{\epsilon_i}\\&=\beta_i\Pi_i-\frac{\beta_i^2\Pi_i^2}{\epsilon_i}+\frac{\beta_i(\beta_i-\hat{\beta}_i)\Pi_i^2}{\epsilon_i}\\&\le\frac{\epsilon_i}{4}+\frac{\beta_i\left(v_{p_i}(T_j^{p_i})-v_{p_i}(t)\right)\Pi_i^2}{\epsilon_i}.\end{aligned}\tag{22}$$

Note that

$$\begin{aligned}&\chi_{i,2}+\frac{\beta_i\left(v_{p_i}(T_j^{p_i})-v_{p_i}(t)\right)\Pi_i^2}{\epsilon_i}\\\overset{(19)}{=}&\beta_i\Big[(h_i+\kappa_i)\left(v_{p_i}(T_j^{p_i})-v_{p_i}(t)\right)\\&+\left(a_{p_i}(T_j^{p_i})-a_{p_i}(t)\right)+\frac{1}{\epsilon_i}\left(v_{p_i}(T_j^{p_i})-v_{p_i}(t)\right)\Pi_i^2\Big]\\\overset{(4)}{\le}&\frac{\kappa_i}{2}\beta_i^2+\frac{1}{2\kappa_i}\left[\left(\frac{h_i+\kappa_i}{\phi_{p_i,1}}\right)^2+\left(\frac{1}{\phi_{p_i,2}}\right)^2\right.\\&\left.+\left(\frac{1}{\epsilon_i\phi_{p_i,3}}\right)^2\right]\left\|\boldsymbol{\Phi}_{p_i}\boldsymbol{\xi}_{p_i}^{\mathrm{T}}\right\|^2\\\overset{(5)}{\le}&\frac{\kappa_i}{2}\beta_i^2+\varpi_i\zeta_{p_i}^2,\end{aligned}\tag{23}$$

where

$$\varpi_i=\frac{1}{2\kappa_i}\left[\left(\frac{h_i+\kappa_i}{\phi_{p_i,1}}\right)^2+\left(\frac{1}{\phi_{p_i,2}}\right)^2+\left(\frac{1}{\epsilon_i\phi_{p_i,3}}\right)^2\right].\tag{24}$$

By substituting inequalities (22) and (23) into Eq. (17), we have

$$\dot{V}_i\le-\frac{\kappa_i}{2}\beta_i^2+\varpi_i\zeta_{p_i}^2+\frac{\epsilon_i}{4}.\tag{25}$$

According to inequalities (21) and (25), for any $|\mu_i|$, we have

$$\begin{aligned}\dot{V}_i&\le-\frac{\kappa_i}{2}\beta_i^2+\varpi_i\zeta_{p_i}^2+\frac{\epsilon_i}{4}\\&=-\frac{\kappa_i}{2}\beta_i^2+\varkappa_i,\end{aligned}\tag{26}$$

where $\varkappa_i=\varpi_i\zeta_{p_i}^2+\dfrac{\epsilon_i}{4}$.

Because κ_i, ϖ_i, ζ_{p_i}, and ϵ_i are positive scalar constants according to their definitions above, $\varkappa_i$ is also a positive scalar constant. Therefore, according to inequality (26), $\dot{V}_i$ is negative definite for all $|\beta_i|>\sqrt{2\varkappa_i/\kappa_i}$. This means that the controlled system renders uniform boundedness and uniform ultimate boundedness of β_i referring to the standard arguments in Yu et al. (2019). Furthermore, the uniform boundedness (Definition 1) follows with

$$R_i=\sqrt{\frac{2\varkappa_i}{\kappa_i}},\ \chi_i(y_i)=\begin{cases}R_i, & \text{if } y_i\le R_i,\\ y_i, & \text{otherwise.}\end{cases}\tag{27}$$

The uniform ultimate boundedness (Definition 2) also follows with

$$\underline{\chi}_i=R_i,\ T_i(\overline{\chi}_i,y_i)=\begin{cases}0, & \text{if } y_i\le\overline{\chi}_i,\\ \dfrac{y_i^2-\overline{\chi}_i^2}{\overline{\chi}_i^2-R_i^2}, & \text{otherwise.}\end{cases}\tag{28}$$

According to Definition 2 and Eq. (28), the lumped error $\beta_i(t)$ will be eliminated and stay within a small range $(-\overline{\chi}_i, \overline{\chi}_i)$ in finite time $T_i(\overline{\chi}_i, y_i)$, i.e.,

$$-\overline{\chi}_i \le \beta_i(t) = h_i e_i(t) + \dot{e}_i(t) \le \overline{\chi}_i. \tag{29}$$

Solving the differential inequality (29), we have that for $\forall i \in I$,

$$\begin{cases} e_i(t) \ge -\dfrac{\overline{\chi}_i}{h_i} + \left(e_i(T) + \dfrac{\overline{\chi}_i}{h_i}\right)\exp\big(-h_i(t-T)\big), \\ e_i(t) \le \dfrac{\overline{\chi}_i}{h_i} + \left(e_i(T) - \dfrac{\overline{\chi}_i}{h_i}\right)\exp\big(-h_i(t-T)\big), \end{cases} \tag{30}$$

where $t > T = \max_{i\in I} T_i(\overline{\chi}_i, y_i)$. Inequality (30) indicates that $e_i(t)$ is uniformly ultimately bounded and T is the boundedness time. Referring to Definition 3, the virtual platoon is proved to be string-stable.

Remark 3 As mentioned in Section 2.2, the cooperation problem for a generic conflicting scenario can be transformed into a virtual platoon formation and control problem that relies solely on the 1D distance from the intersection and vehicle motion information. In other words, the proposed controller can be flexibly deployed in real-world situations without any algorithmic change.

5 Simulation and experimental results

The effectiveness of the proposed method is evaluated both in simulations and experiments. Section 5.1 presents the simulation setup and results. Section 5.2 presents the experimental setup and results.

5.1 Simulation setup and results

In this subsection, simulations based on the conflicting scenario shown in Fig. 1a are conducted in MATLAB. The communication range of the prescribed intersection is 75 m. The 1st and 6th vehicles are multi-purpose vehicles (MPVs). The 2nd, 3rd, and 5th vehicles are sedans. The 4th vehicle is a truck. Table 1 lists the parameters associated with triggering conditions, vehicle dynamics, and controller parameters. Moreover, we adopt trigonometric functions to mimic practical uncertainties of vehicle dynamics. The corresponding frequency coefficients are randomly chosen from $\{0.1, 0.2, ..., 1\}$. The fixed transmission period is $h = 0.1$ s. It is assumed that the transmission in the TTC scheme is executed every 0.1 s while that in the ETC scheme is checked every 0.1 s and is executed only if the triggering condition is met.

Fig. 2a presents the vehicles' arrival time and initial speed. Different colors correspond to the different vehicle types. It is assumed that the conflict-free passing sequence of these six vehicles is determined based on the algorithm by Xu et al. (2018) and the results are shown in Fig. 2b. According to Fig. 2b, the 1st, 2nd, 3rd, and 4th vehicles function as predecessors. Therefore, we further explore

Table 1 Simulation parameters

Type	Parameter	Value	Type	Parameter	Value
Triggering condition	$\phi_{i,1},\ \phi_{i,2},\ \phi_{i,3}$	0.9, 0.5, 0.1	Car-following model	q_i	0.5
	ζ_i	0.15		d_s	5 m
Input delay	τ_i (sedan)	0.5	Controller parameter	h_i	0.22
	τ_i (MPV)	0.5		κ_i	0.1
	τ_i (truck)	0.6		ϵ_i	5
Nominal vehicle mass	M_i (sedan)	950 kg	Vehicle length	L_i (sedan)	4 m
	M_i (MPV)	1000 kg		L_i (MPV)	4 m
	M_i (truck)	1860 kg		L_i (truck)	5.3 m
Nominal aerodynamics	$\bar{c}_i$ (sedan)	0.5 N· s^2/m^2	Uncertain portion	Δc_i (Sedan)	$0.2\sin(\xi_i t)$
	$\bar{c}_i$ (MPV)	0.5 N· s^2/m^2		Δc_i (MPV)	$0.22\sin(\xi_i t)$
	$\bar{c}_i$ (truck)	0.8 N· s^2/m^2		Δc_i (truck)	$0.4\sin(\xi_i t)$
Nominal road resistance	$\bar{f}_i$ (sedan)	180 N	Uncertain portion	Δf_i (Sedan)	$110\cos(\xi_i t)$
	$\bar{f}_i$ (MPV)	200 N		Δf_i (MPV)	$120\cos(\xi_i t)$
	$\bar{f}_i$ (truck)	400 N		Δf_i (truck)	$220\cos(\xi_i t)$
Assumption 1	$\Pi_i(a_i, v_i, t) = 0.003v_i^2 + 0.0015 v_i a_i + 1.2$				

MPV: multi-purpose vehicle

the transmission between these vehicles and their followers.

Fig. 3 shows the transmission instants and release time intervals of the aforementioned four predecessors. It can be seen that the distribution of triggering time is consistent with the speed history of the vehicles as shown in Fig. 4b. The triggering time is concentrated in the initial stage and the speed variation stage (8–16 s). Besides, the triggering time distribution of vehicles with different passing sequences exhibits a "delayed" effect. For example, the 1st vehicle encounters the intensive triggering stage from 0 s when it enters the intersection. The intensive triggering stage of the 2nd, 3rd, and 4th vehicles delays for about 2 s compared with that of the 1st vehicle. The number of transmissions, transmission ratio, and reduced number of transmissions for data are listed in Table 2. It can be seen that an average of 77 sampled data packets need to be transmitted via the VANET within the cooperation area. All 200 sampled data packets will be transmitted via the VANET during the cooperation process

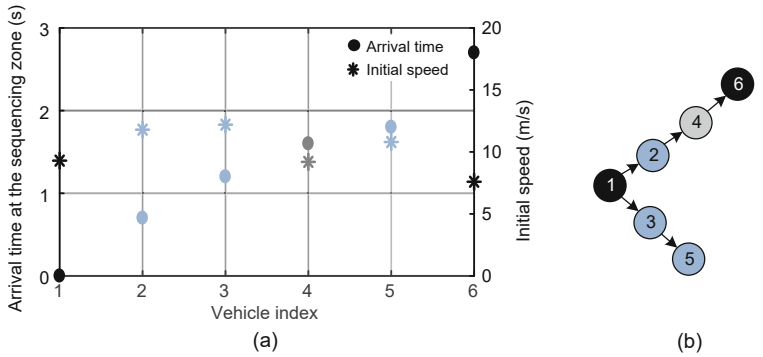

Fig. 2 Initial information of approaching vehicles: (a) arrival time and initial speed; (b) conflict-free passing sequence. References to color refer to the online version of this figure

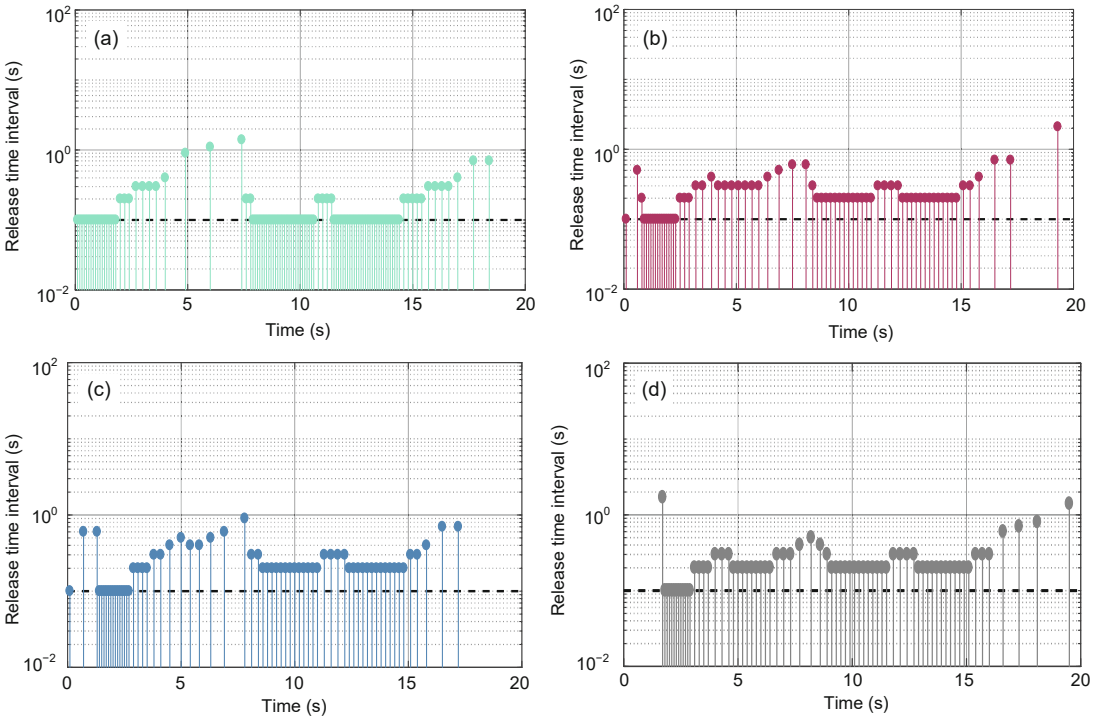

Fig. 3 Transmission instants and release time intervals in the simulations: (a) 1st vehicle; (b) 2nd vehicle; (c) 3rd vehicle; (d) 4th vehicle

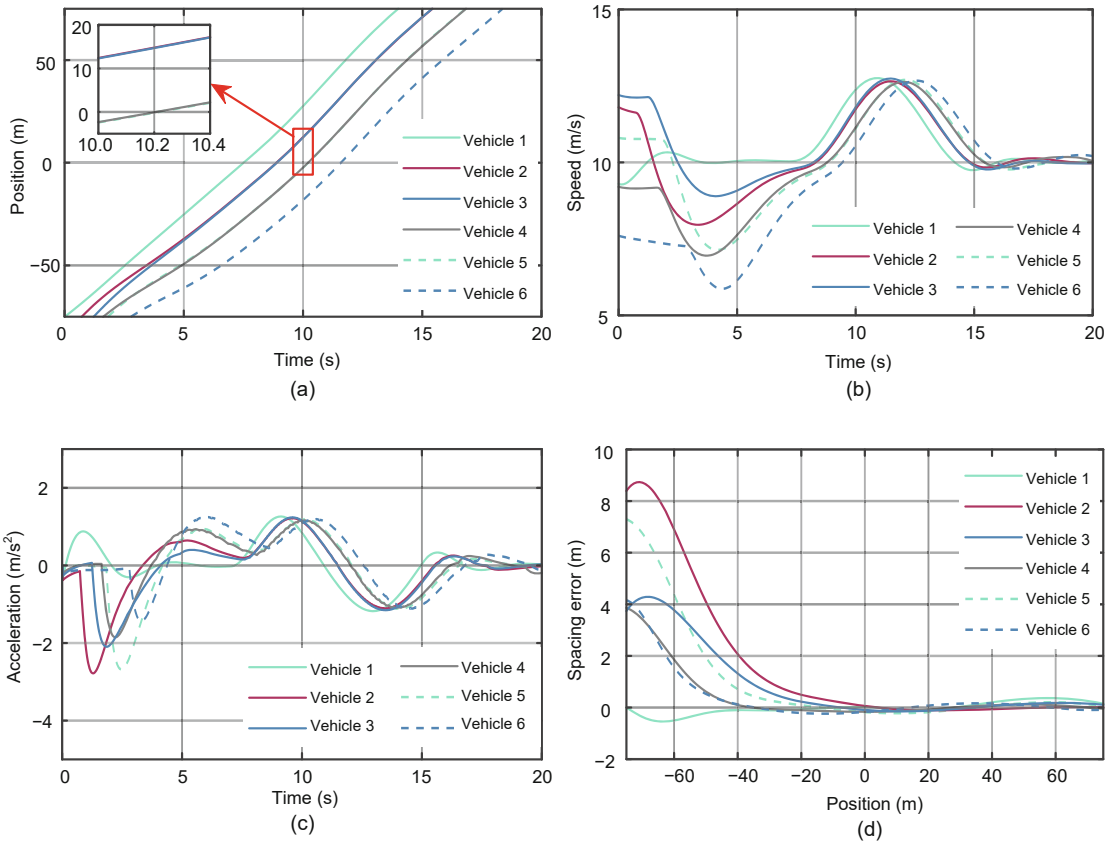

Fig. 4 Results of vehicle motion: (a) position; (b) speed; (c) acceleration; (d) spacing error. References to color refer to the online version of this figure

if the TTC method is adopted. In summary, the proposed method reduces the number of transmissions by 61.5% on average compared with the TTC method.

Fig. 4 presents the state history of the vehicles. The passing sequence is well executed according to the position history shown in Fig. 4a; i.e., vehicles without conflicts pass the intersection together and vehicles with a conflict relationship pass in succession with a prescribed spacing (the partial enlarged view in Fig. 4a). Moreover, the speed history (Fig. 4b) echoes the data transmission instants in Fig. 3. When the speed fluctuation occurs (8–16 s), the predecessors have to inform their followers, and hence the transmission is more intensive during this time. Additionally, the absolute value of the maximum acceleration is less than 3 m/s^2 according to Fig. 4c. Last but not least, the spacing error is eliminated when vehicles arrive at the conflicting area as shown in Fig. 4d, which validates the safety of the cooperation process with the proposed method.

5.2 Experimental setup and results

The proposed ETC is validated in Expo Park in Qingdao, China, using two autonomous tractor trucks at the intersection. The test vehicles are JH6 trucks supplied by the China FAW Group Corporation.

The experimental setup is illustrated in Fig. 5. Fig. 5a exhibits a snapshot of the cooperation process. The 1st vehicle is making a left turn and its path is shown by the white line. The 2nd vehicle is driving straight and its path is shown by the orange line. In particular, the 2nd vehicle follows the 1st vehicle and they form a virtual platoon. The on-board equipment and software architecture are shown in Fig. 5b. Both vehicles are equipped with drive-by-wire chassis and are capable of path tracking with on-board active steering systems. The control algorithm is conducted on NVIDIA Jeton TX2 Autobox. The position of each vehicle is measured by a global navigation satellite system (GNSS), which has

Table 2 Simulation results

Vehicle index	Number of transmissions	Transmission ratio	Reduced number of transmissions
1	105	52.5%	95
2	72	36.0%	128
3	69	34.5%	131
4	62	31.0%	138

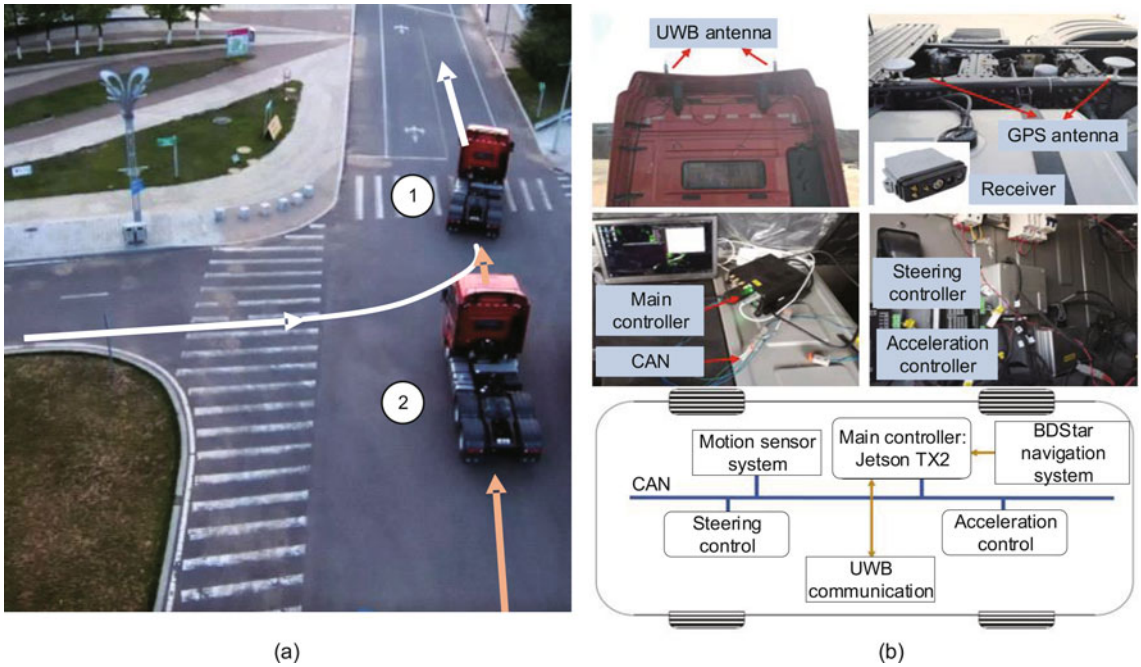

Fig. 5 Experimental setup: (a) virtual platoon; (b) on-board hardware and software of test vehicles. UWB: ultra-wide bandwidth; GPS: Global Positioning System; CAN: controller area network. References to color refer to the online version of this figure

centimeter-level accuracy. The V2V communication is executed by ultra-wide bandwidth (UWB). Fig. 5b shows the software architecture of the truck. The data are transmitted at each time instant in the experiments. However, a triggering module is embedded in the main controller to ensure that the data are refreshed only if the triggering condition is satisfied. Otherwise, the data stay the same by a zero-order holder (ZOH). Therefore, by analyzing the transmission data history, we can obtain the number of transmissions in the event-triggered communication scheme.

We design four cases to test the proposed method, where we vary the speed profile of the predecessor. The speed history of the vehicles is shown in Fig. 6a. The 2nd vehicle follows its predecessor well. Furthermore, the tracking performance shown in Figs. 6b and 6c verifies the effectiveness of the proposed method. The speed errors in all four cases are extremely low, which indicates the remarkable tracking performance. The fluctuation in speed error during the acceleration and deceleration stages is caused by the time delay of the automated manual transmission (AMT). The spacing error is smaller than 3 m when the speed of the 1st vehicle is steady (i.e., in cases 1–3). The severe acceleration and deceleration and a high speed (55 km/h) in case 4 lead to a relatively large spacing error. Considering that vehicles approaching the conflicting scenario tend to drive steadily at a relatively low speed (just like the speed profile in cases 1–3), the proposed method is hence ready for practical implementation.

Fig. 7 shows the transmission instants and release time intervals of the test vehicles. Transmission instants are concentrated in the acceleration and deceleration stages, which corresponds with the definition of the triggering condition in Eq. (4). Transmission instants are sparse when the vehicle drives at a

uniform speed. Detailed analysis for the number of transmissions is shown in Table 3. In the four cases, the proposed ETC method can reduce the number of transmissions by 74.4% on average compared with the TTC method.

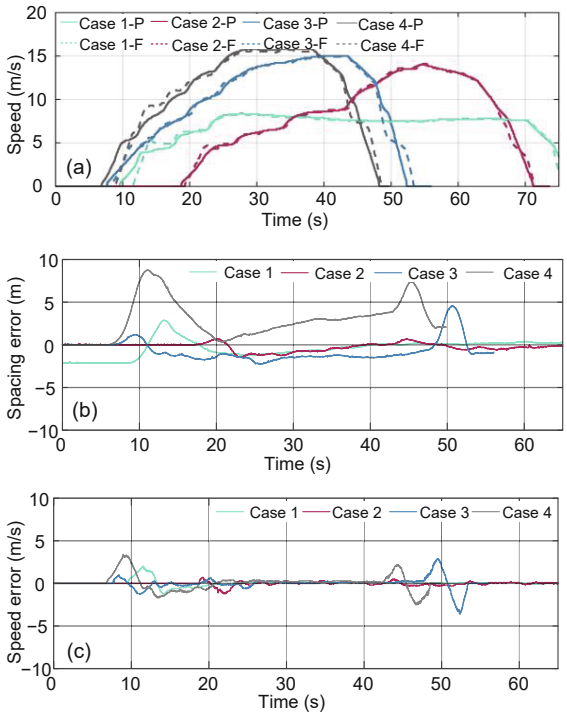

Fig. 6 Vehicle motion and tracking performance: (a) speed; (b) spacing error; (c) speed error. P: predecessor; F: follower. References to color refer to the online version of this figure

In summary, it can be concluded that the proposed distributed event-triggered robust control is capable of coordinating multiple CAVs in conflicting scenarios. Detailed performance is threefold. First, the proposed method is based on the event-triggered communication scheme, and hence can significantly reduce the use of communication resources compared with TTC methods, which improves communication performance. Second, the triggering condition in the proposed method fuses the state error with parametric uncertainty, which has not been proposed or explored in existing ETC studies. Third, the effectiveness of the proposed method is validated in the simulations and experiments, and the results indicate that it is readily applicable.

6 Conclusions

In this paper, the multi-vehicle coordination problem in conflicting scenarios has been studied from a communication-resource-aware and robust perspective. After forming a virtual lane by projection, the conflict passing sequence can be determined. On this basis, we have provided distributed event-triggered control for the multi-vehicle

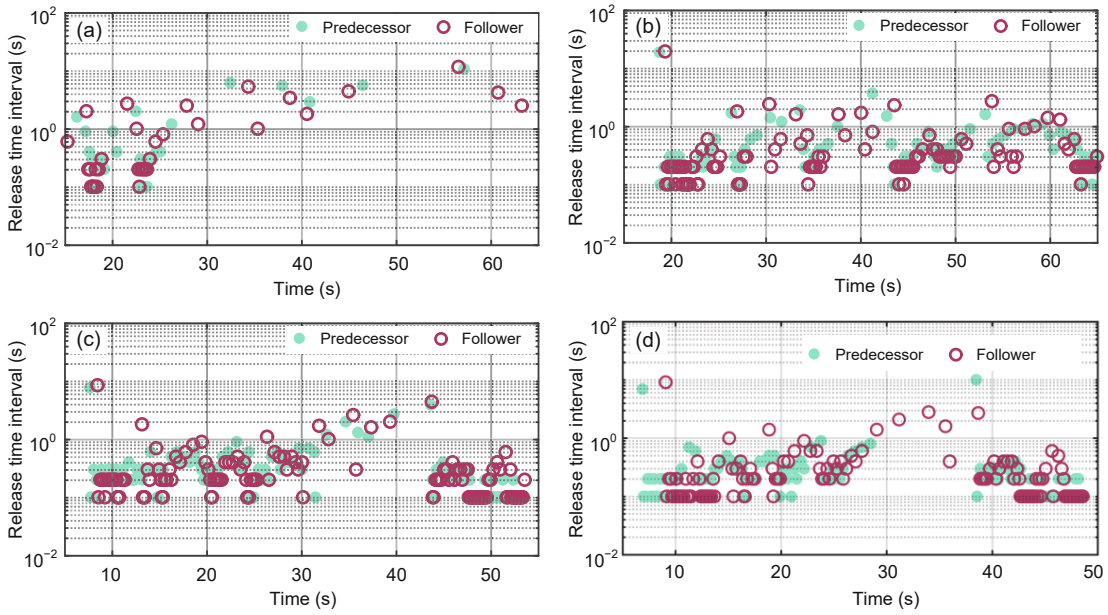

Fig. 7 Transmission instants and release time intervals in the experiments: (a) case 1; (b) case 2; (c) case 3; (d) case 4

Table 3 Experimental results

Case index	Vehicle	Number of transmissions	Transmission ratio	Reduced number of transmissions
1	Predecessor	86	17.2%	414
	Follower	89	17.8%	411
2	Predecessor	129	25.8%	371
	Follower	140	28.0%	360
3	Predecessor	134	26.8%	366
	Follower	138	27.6%	362
4	Predecessor	144	32.0%	306
	Follower	132	29.3%	318

cooperation problem. Most notably, we have presented a novel triggering condition that fuses the state error with parametric uncertainty. The uniform boundedness, uniform ultimate boundedness, and string stability of the controlled system have been theoretically proved using the Lyapunov stability theory, and simulation and experimental results verified the effectiveness of the proposed method. It is worth stressing that the proposed method reduced the number of transmissions by 61.5% and 74.4% on average in simulations and experiments, respectively, compared with TTC methods. In summary, the proposed method achieved communication-efficient and collision-free cooperation in conflicting scenarios.

Future research can be conducted to design an optimal triggering threshold to balance tracking performance and communication efficiency. The threshold in the triggering condition is constant. In future work, an adaptive law can be developed for the dynamic threshold. Additionally, the feasibility of the proposed control method should be explored at high driving speeds and under severe speed changes.

Contributors

Yifan JIA and Jin HUANG designed the research. Zhanyi HU and Yingjun QIAO processed the data and drafted the paper. Xingyu LI helped organize the paper. Zhanyi HU, Yingjun QIAO, and Zhihua ZHONG revised and finalized the paper.

Compliance with ethics guidelines

Zhanyi HU, Yingjun QIAO, Xingyu LI, Jin HUANG, Yifan JIA, and Zhihua ZHONG declare that they have no conflict of interest.

References

Bian YG, Li SE, Ren W, et al., 2020. Cooperation of multiple connected vehicles at unsignalized intersections: distributed observation, optimization, and control. *IEEE Trans Ind Electron*, 67(12):10744-10754. https://doi.org/10.1109/TIE.2019.2960757

Castiglione LM, Falcone P, Petrillo A, et al., 2021. Cooperative intersection crossing over 5G. *IEEE/ACM Trans Netw*, 29(1):303-317. https://doi.org/10.1109/TNET.2020.3032652

Chen YH, Zhang XR, 2010. Adaptive robust approximate constraint-following control for mechanical systems. *J Franklin Inst*, 347(1):69-86. https://doi.org/10.1016/j.jfranklin.2009.10.012

Dai PL, Liu K, Zhuge QF, et al., 2016. Quality-of-experience-oriented autonomous intersection control in vehicular networks. *IEEE Trans Intell Transp Syst*, 17(7):1956-1967. https://doi.org/10.1109/TITS.2016.2514271

di Bernardo M, Salvi A, Santini S, 2015. Distributed consensus strategy for platooning of vehicles in the presence of time-varying heterogeneous communication delays. *IEEE Trans Intell Transp Syst*, 16(1):102-112. https://doi.org/10.1109/TITS.2014.2328439

Ding L, Han QL, Ge XH, et al., 2018. An overview of recent advances in event-triggered consensus of multiagent systems. *IEEE Trans Cybern*, 48(4):1110-1123. https://doi.org/10.1109/TCYB.2017.2771560

di Vaio MD, Falcone P, Hult R, et al., 2019. Design and experimental validation of a distributed interaction protocol for connected autonomous vehicles at a road intersection. *IEEE Trans Veh Technol*, 68(10):9451-9465. https://doi.org/10.1109/TVT.2019.2933690

Dolk V, Heemels M, 2017. Event-triggered control systems under packet losses. *Automatica*, 80:143-155. https://doi.org/10.1016/j.automatica.2017.02.029

Dolk VS, Ploeg J, Heemels MPMH, 2017. Event-triggered control for string-stable vehicle platooning. *IEEE Trans Intell Transp Syst*, 18(12):3486-3500. https://doi.org/10.1109/TITS.2017.2738446

Dresner K, Stone P, 2008. A multiagent approach to autonomous intersection management. *J Artif Intell Res*, 31(1):591-656. https://doi.org/10.5555/1622655.1622672

Ge XH, Han QL, Zhang XM, 2018. Achieving cluster formation of multi-agent systems under aperiodic sampling and communication delays. *IEEE Trans Ind Electron*, 65(4):3417-3426. https://doi.org/10.1109/TIE.2017.2752148

Guo G, Ding L, Han QL, 2014. A distributed event-triggered transmission strategy for sampled-data consensus of multi-agent systems. *Automatica*, 50(5):1489-1496. https://doi.org/10.1016/j.automatica.2014.03.017

Huang S, Sadek AW, Zhao YJ, 2012. Assessing the mobility and environmental benefits of reservation-based intelligent intersections using an integrated simulator. *IEEE Trans Intell Transp Syst*, 13(3):1201-1214. https://doi.org/10.1109/TITS.2012.2186442

Li SE, Zheng Y, Li KQ, et al., 2017. Dynamical modeling and distributed control of connected and automated vehicles: challenges and opportunities. *IEEE Trans Intell Transp Syst*, 9(3):46-58. https://doi.org/10.1109/MITS.2017.2709781

Li T, Wen CY, Yang J, et al., 2020. Event-triggered tracking control for nonlinear systems subject to time-varying external disturbances. *Automatica*, 119:109070. https://doi.org/10.1016/j.automatica.2020.109070

Li W, Ban XG, 2020. Connected vehicle-based traffic signal coordination. *Engineering*, 6(12):1463-1472. https://doi.org/10.1016/j.eng.2020.10.009

Meng Y, Li L, Wang FY, et al., 2018. Analysis of cooperative driving strategies for nonsignalized intersections. *IEEE Trans Veh Technol*, 67(4):2900-2911. https://doi.org/10.1109/TVT.2017.2780269

Mirheli A, Tajalli M, Hajibabai L, et al., 2019. A consensus-based distributed trajectory control in a signal-free intersection. *Transp Res Part C Emerg Technol*, 100:161-176. https://doi.org/10.1016/j.trc.2019.01.004

Morales Medina AI, van de Wouw N, Nijmeijer H, 2018. Cooperative intersection control based on virtual platooning. *IEEE Trans Intell Transp Syst*, 19(6):1727-1740. https://doi.org/10.1109/TITS.2017.2735628

Rios-Torres J, Malikopoulos AA, 2017. A survey on the coordination of connected and automated vehicles at intersections and merging at highway on-ramps. *IEEE Trans Intell Transp Syst*, 18(5):1066-1077. https://doi.org/10.1109/TITS.2016.2600504

Shen H, Wang Y, Xia JW, et al., 2019. Fault-tolerant leader-following consensus for multi-agent systems subject to semi-Markov switching topologies: an event-triggered control scheme. *Nonl Anal Hybr Syst*, 34:92-107. https://doi.org/10.1016/j.nahs.2019.05.003

Shi YJ, Han QM, Shen WM, et al., 2021. A multi-layer collaboration framework for industrial parks with 5G vehicle-to-everything networks. *Engineering*, 7(6):818-831. https://doi.org/10.1016/j.eng.2020.12.021

Uno A, Sakaguchi T, Tsugawa S, 1999. A merging control algorithm based on inter-vehicle communication. Proc IEEE/IEEJ/JSAI Int Conf on Intelligent Transportation Systems, p.783-787. https://doi.org/10.1109/ITSC.1999.821160

Wen SX, Guo G, Chen B, et al., 2018. Event-triggered cooperative control of vehicle platoons in vehicular ad hoc networks. *Inform Sci*, 459:341-353. https://doi.org/10.1016/j.ins.2018.02.051

Xu B, Li SE, Bian YG, et al., 2018. Distributed conflict-free cooperation for multiple connected vehicles at unsignalized intersections. *Transp Res Part C Emerg Technol*, 93:322-334. https://doi.org/10.1016/j.trc.2018.06.004

Yu RR, Chen YH, Zhao H, et al., 2019. Self-adjusting leakage type adaptive robust control design for uncertain systems with unknown bound. *Mech Syst Signal Process*, 116:173-193. https://doi.org/10.1016/j.ymssp.2018.06.031

Yue W, Wang LY, Guo G, 2017. Event-triggered platoon control of vehicles with time-varying delay and probabilistic faults. *Mech Syst Signal Process*, 87:96-117. https://doi.org/10.1016/j.ymssp.2016.09.042

Zheng Y, Li SE, Wang JQ, et al., 2016. Stability and scalability of homogeneous vehicular platoon: study on the influence of information flow topologies. *IEEE Trans Intell Transp Syst*, 17(1):14-26. https://doi.org/10.1109/TITS.2015.2402153